

A CMOS integrated impedance-to-frequency converter for sensing cellular adhesion

A. Mucha^{1,2}, M. Schienle¹, and D. Schmitt-Landsiedel²

¹Corporate Research and Technologies, Siemens AG, Munich, Germany

²Lehrstuhl für Technische Elektronik, Technische Universität München, Munich, Germany

Abstract. Sensing cellular adhesion via impedance measurements provides a versatile and easily accessible means for monitoring in-vitro cell cultures. Previous works used external electronics connected via cables to microelectrodes to achieve this goal, thus incurring parasitic impedance, electromagnetic interference, and bulky measurement setups. In this work we present a CMOS impedance-to-frequency converter integrated with biocompatible planar surface electrodes to make a compact and robust sensor chip for in-vitro cell monitoring. The system features an 8×8 array of individually addressable electrodes connected to four impedance-to-frequency converter circuits with externally adjustable biasing and square wave output. We present first measurement results obtained with the integrated electronics that demonstrate the successful operation of the system and show good agreement with models of the electrode and cell impedances.

1 Introduction

Quick and reliable information about the presence of bioactive substances in water can be vital in many situations. From developing countries, where infrastructure for drinking water might be nonexistent or unreliable, to modern waste water recycling facilities, often the question is not primarily which specific substances are in the water, but rather simply if it is safe to consume, i.e. if it has any negative effects on the human organism. Although chemical analysis technology has now reached a maturity which allows the detection of a wide range of specific contaminants with high sensitivity, it is impractical to test for all relevant substances. Chemical analyses by their nature also cannot give information on the biological activity of substances. This is the strength of biosen-

sors, which combine biological elements with an electronic readout device to measure the reaction of living systems to a stimulus. Cells cultured "in-vitro" react to stimuli much the same way as in the whole organism ("in-vivo"). Thus whole cell biosensors using mammalian or human cell lines are a promising avenue to create a water monitoring system with a high validity as an indicator of bioactive contaminants. Cells can be cultured on sensor chips equipped with transducers for various physical and chemical parameters such as impedance, oxygen concentration and acidity to monitor cell health and metabolism (Bousse, 1996). In this paper, we focus on the measurement of impedance as an indicator of cell morphology and adhesion. It is a valuable parameter for the assessment of cell reactions because it is very fast and many substances cause morphological changes in cells (Wegener et al., 2000).

Previously published whole cell sensor systems used passive chips connected to external electronics. This is problematic because the signals generated by the transducers are very weak, making the systems susceptible to noise and interference. The use of CMOS technology to integrate the transducers with on-chip electronics offers a great advantage in this regard because the reduced physical distance between the sensing elements and the front end amplifier circuitry translates into reduced parasitic impedance, interference and noise. On-chip analog-to-digital conversion and data multiplexing also reduce the number of external connections and thus further improve the robustness.

2 Principle of cell impedance measurement

Animal cells have a phospholipid bilayer membrane to separate the interior from the exterior of the cell. Electrically, this membrane is mainly an insulator, as it does not allow the passage of charge except through ion channels embedded in it. This results in an electrical behavior which can



Correspondence to: A. Mucha
(andreas.mucha@mytum.de)

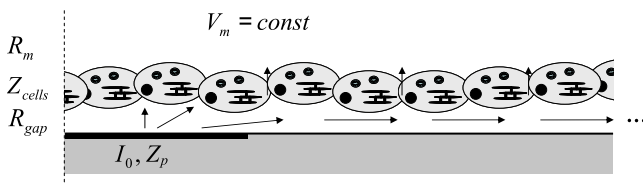


Fig. 1. Schematic cross section of a cell monolayer, having a distributed impedance Z_{cells} , growing on the sensor. A current I_0 is injected into the sensing electrode with polarization impedance Z_p on the left and spreads in the space under the cells and between the cells into the bulk medium, which is assumed to be at a fixed potential V_m . The dashed line at the left indicates the axis of symmetry.

be modeled as a parallel RC circuit. Published values of the cell membrane impedance are around 1–2 k Ω cm² and 1–4 μ Fcm⁻² (Ritter et al., 1990; Ehret et al., 1997; Lo et al., 1995). Culture media used to grow cells contain various ions in concentrations similar to those in the original organism, giving them a relatively low resistivity of around 65 Ω cm.

If a small current is applied to the medium by means of electrodes on the surface of the sensor chip, a low resistance (voltage drop) will consequently be measured in the absence of cells. If cells are however present on the chip or even the electrodes themselves, a larger voltage drop will arise due to their higher impedance. This effect is amplified when the cells are growing as a confluent monolayer, as the current is then mostly constrained to a narrow gap under the cell layer. In this case, even small morphological changes of the cells can result in a large change of the collective impedance of the cell layer as the tightness of the junctions between the cells varies and current can escape into the bulk medium above them more or less easily. The various paths the current can take are illustrated in Fig. 1.

2.1 Electrode impedance

If one of the electrodes has a much larger area than the others, it acts as a counter electrode which keeps the bulk electrolyte at a fixed potential. Its impedance can be neglected in this case. The other electrodes with the smaller area, which we will call sensing electrodes, however present a significant impedance which is added to the useful signal represented by the cell impedance. In Fig. 2, the components of the electrode impedance are shown: The charge transfer resistance R_{ct} represents the passage of charge carriers between the metal and the electrolyte. As the redox reactions involved in this process need some activation energy, its value depends on the applied voltage to the electrode. In the case of a cell impedance sensor, electrochemical reactions are undesired as they corrupt the electrodes. Thus only very small excitations can be applied to the electrodes and the charge transfer resistance can be considered infinite.

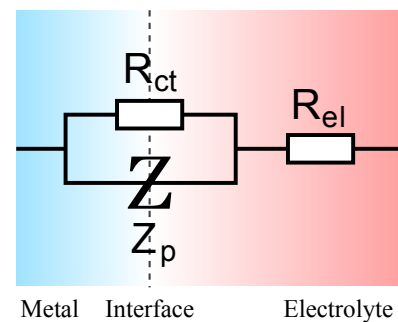


Fig. 2. Equivalent circuit diagram of a metal electrode in contact with an electrolyte.

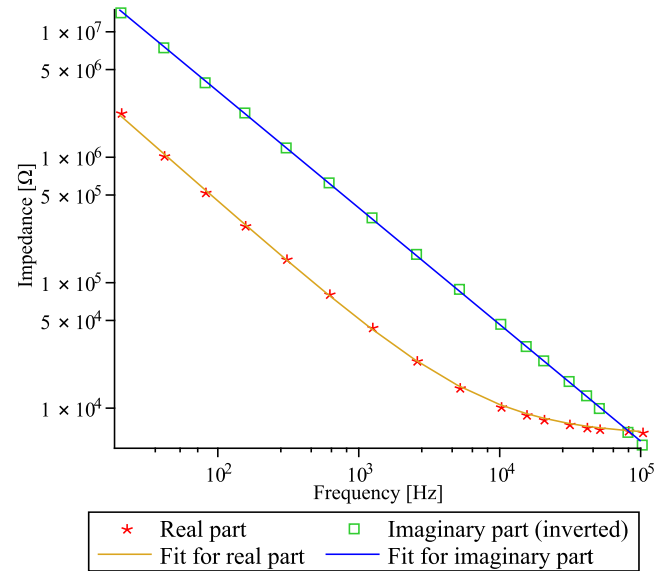


Fig. 3. Typical impedance spectrum of a gold electrode in cell culture medium.

This leaves the polarization impedance Z_p as the only element between metal and electrolyte. It can be modeled phenomenologically by the equation

$$Z_p = Af^{-\alpha} - jBf^{-\beta} \quad (1)$$

with the complex impedance Z_p in ohms and A , B , α and β positive constants (Ragheb and Geddes, 1991). As the frequency f approaches zero, the real and imaginary parts of the polarization impedance go towards positive and negative infinity, respectively, so no DC current can pass through it. In series with the polarization impedance is the spreading resistance through the medium R_{el} , which must thus be added to the total impedance (Franks et al., 2005).

In Fig. 3, a typical impedance spectrum of one of the electrodes on our chip is shown. The real part of the impedance is represented by the asterisk symbols, and the imaginary part (with inverted sign) by the squares. Also shown is our best fit of the Eq. (1) to the data, with the addition of a real constant term for the spreading resistance. Its value was extracted

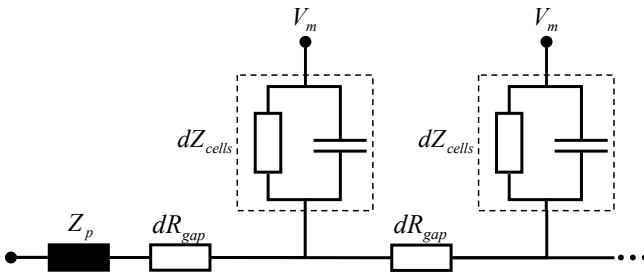


Fig. 4. Simplified schematic of distributed cell impedance.

as $6 \text{ k}\Omega$. The exponents for the real and imaginary parts of the polarization impedance are $\alpha = 0.99$ and $\beta = 0.93$, respectively, and their constant factors $A = 4.23 \times 10^7$ and $B = 2.43 \times 10^8$. Since the imaginary part is dominant in Z_p and its frequency dependence is close to that of an ideal capacitance, i.e. $\beta = -1$, the polarization impedance can be approximated to first order as a capacitance.

2.2 Cell layer impedance

The impedance of a cell layer growing on the chip is unfortunately not as easy to model. A simplified schematic of the cell impedance, corresponding to the geometry in Fig. 1, is depicted in Fig. 4. The constriction resistance R_{gap} of the space under the cells and the cells themselves form a distributed impedance which in the one-dimensional case resembles a transmission line structure. A complete model of the cell impedance Z_{cells} has to take into account both the capacitive behavior of the cell membrane and the resistive paths, which can be either through ion channels and the cytosol or through gaps between the cells. However, the capacitive coupling through the cells in general only becomes noticeable at frequencies significantly above 10 kHz, so the cell impedance can be approximated as a pure resistance R_{cells} at lower frequencies.

For the one-dimensional case, i.e. restricting the analysis to geometries with axial symmetry and using some assumptions, analytical models can be derived (Lo et al., 1995; Urdapilleta et al., 2006). For other geometries, numerical methods such as finite elements modeling (FEM) have to be used. We thus used ANSYS finite elements software to evaluate various electrode layouts and to optimize the electrode sizes. Values for the cell layer resistance and typical heights of the cell-substrate gap were obtained from published literature (*ibid.*). Especially the gap height h is a critical parameter, since it directly influences the constriction resistance of the cell layer and thus the useful signal. The published values in excess of 1 μm that were extracted using the previously mentioned analytical models however seem greatly exaggerated compared to actual measurements (Braun and Fromherz, 1998), so we explored the relationship between h and the expected impedance in a series of simulations.

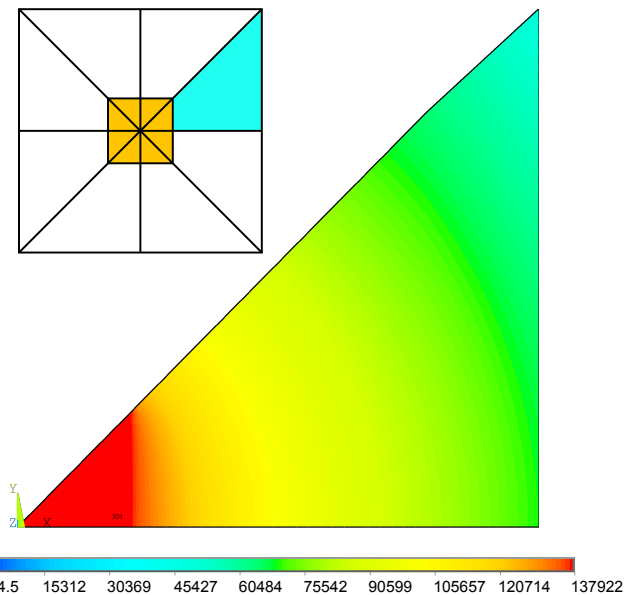


Fig. 5. Top view of voltage distribution in the gap under the cells ($h = 2 \mu\text{m}$) simulated for an imposed current of 1 A. The insert in the upper left shows the segmentation of the finite elements model into eight identical sectors.



Fig. 6. Cross section of finite elements model along XZ-plane. Blue elements represent the cell layer, red elements cell culture medium.

The simulated geometry in top view is depicted in Fig. 5. A square electrode (modeled as an equipotential region) is located in the center of the simulation space, which has a boundary condition for far field decay imposed, thus simulating an infinitely large counter electrode at infinite distance. By exploiting the symmetries of the geometry, only a sector of 1/8 of the space needs to be simulated. A cross section of the model, showing the gap, the cell layer and the bulk medium above it, is depicted in Fig. 6. The arrows on the left indicate the area where the electrode current is impressed.

Examination of the simulated current distribution revealed that the current indeed spreads mostly in the gap under the cells. One could thus assume that the spreading resistance can be described by an equation of the form

$$R_{\text{gap}}(h) = F_{\text{geom}} \frac{\rho}{h} \quad (2)$$

with F_{geom} as a factor describing the geometry (e.g. electrode area and shape), gap height h and the medium resistivity ρ . A plot of R_{gap} over $1/h$ should thus yield a straight line. However, a significant spreading resistance R_0 of several $\text{k}\Omega$ was

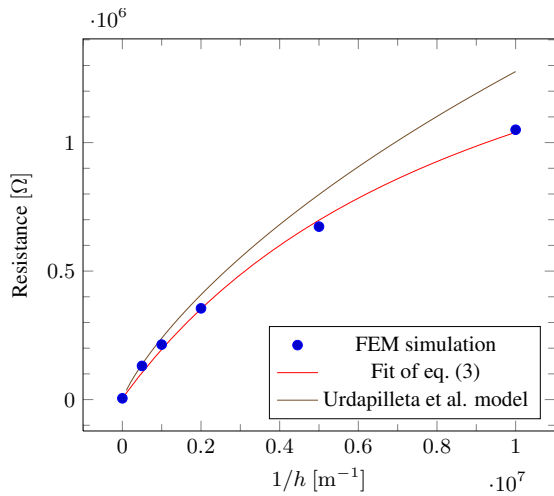


Fig. 7. Plot of cell impedance versus inverse gap height: FEM simulation, fitted curve and analytical model by Urdapilleta et al. for a center electrode of $55 \times 55 \mu\text{m}^2$.

evident in our preliminary measurements even in the absence of cells (see Fig. 3). Some current also does cross the cell layer, mainly directly above the electrode, so the total behavior is better described by the gap resistance in parallel with another resistive term for this direct crossing, i.e. as

$$R_{\text{total}} = R_{\text{gap}}(h) \parallel R_{\text{cells}} + R_0 \quad (3)$$

The plot of the simulated values in Fig. 7 with a superposed fit of Eq. (3) confirms this model. For comparison, the values yielded by application of the Urdapilleta et al. model with the same parameters to a circular electrode of equal area are also plotted.

Summarizing the simulation results, even in the assumed worst case ($h = 2 \mu\text{m}$), the cell layer would present a resistive impedance in excess of $100 \text{ k}\Omega$, a significant increase over the spreading resistance without cells. To separate this useful signal from the background of the electrode impedance, the measurement has to be performed at frequencies around 10 kHz , where the polarization impedance has sufficiently decreased.

3 Impedance-to-frequency converter

Our modeling thus yielded a first-order approximation of the impedance to be measured as a capacitance for the electrode-electrolyte interface in series with a resistance for the cell layer and the medium. Based on this model we developed an integrated circuit to measure the cell impedance. A key aim in the design process was to enable analog-to-digital conversion of cell adhesion data. Thus, an impedance-to-frequency converter was ideally suited, since it only needs an additional counter to directly produce digital values with a wide dynamic range.

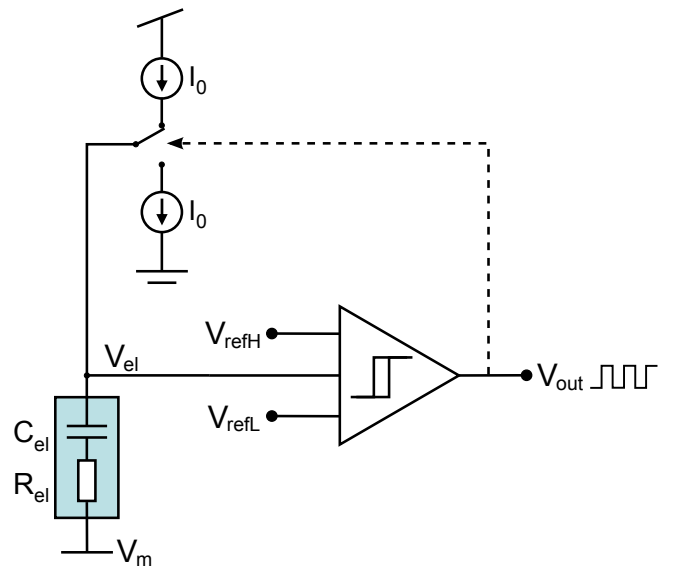


Fig. 8. Simplified block diagram of impedance-to-frequency converter.

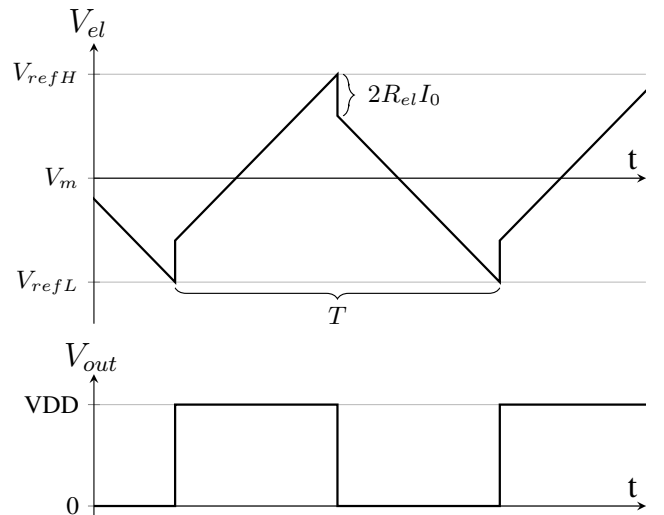


Fig. 9. Idealized plot of the electrode voltage and digital output over time.

3.1 Principle of operation

The measurement principle of our circuit is illustrated by the simplified block diagram in Fig. 8: a surface electrode in contact with the electrolyte is connected to a comparator and a switchable current source. In the shown switch state, the interface capacitance is charged by a constant current I_0 while the comparator senses the electrode potential. As soon as the upper reference voltage V_{refH} is reached, the comparator output V_{out} changes from high to low, which in turn triggers the switch so the electrode is now discharged by $-I_0$. When V_{el} reaches the lower reference voltage V_{refL} , the comparator switches again, completing the cycle. The series resistance

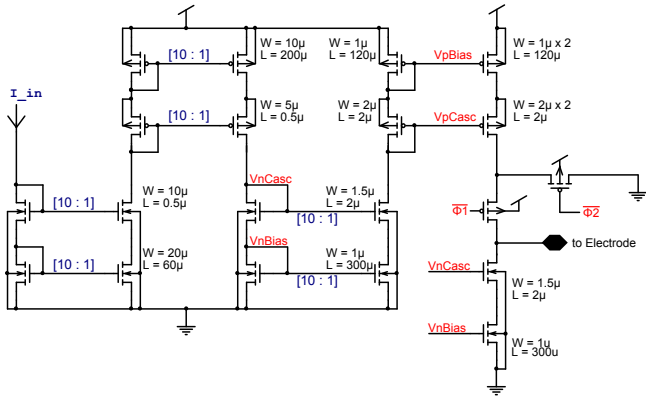


Fig. 10. Schematic of electrode current generator circuit.

R_{el} , constituted either by the spreading resistance or the cell layer, causes an ohmic voltage drop of $R_{el}I_0$ which changes sign at each transition, effectively reducing the voltage window by $2R_{el}I_0$. The period of one charge-discharge cycle as illustrated in Fig. 9 is thus given by

$$T = 2 \frac{C_{el}}{I_0} (\Delta V - 2R_{el}I_0) = 2C_{el} \left(\frac{\Delta V}{I_0} - 2R_{el} \right) \quad (4)$$

with $\Delta V = V_{refH} - V_{refL}$. When cells cover the electrode, increasing R_{el} , the frequency of V_{out} also increases. The output of the comparator thus serves as a digital frequency-modulated signal containing information about cell adhesion.

The same circuit can be connected to an array of sensing electrodes via a switching matrix, accomplishing a spatially resolved measurement of cell adhesion. In order to maximize the long-term stability of the electrodes, redox reactions have to be avoided under all circumstances. This leads to the requirement to limit the polarization voltage of the electrodes to few tens of millivolts. It is also advisable to minimize the electrode current in order to avoid effects like depolarization of the cell membrane, although no exact limits to the current density that cells can be exposed to without harm are known. Surveying published literature about cell impedance measurements led us to the conclusion that a current density of few milliamperes per square centimeter should not be exceeded (Wegener et al., 2000).

These limitations had to be considered in the design of the integrated circuit. They translate into the need for high gain of the comparator to switch at sub-millivolt accuracy while taking steps to mitigate the resulting sensitivity to noise, such as decoupling the reference and supply voltages. The choice of the electrode area needs to strike a balance between the desired high sensitivity to cell adhesion, requiring small electrodes, and the technological limitations as the allowed current decreases with electrode area. With these factors in mind, we designed our sensor for a value of $\Delta V = 20$ mV and the current I_0 adjustable in a range of 10–100 nA.

Accurately generating currents of this magnitude and reliably transporting them to the electrode requires consideration

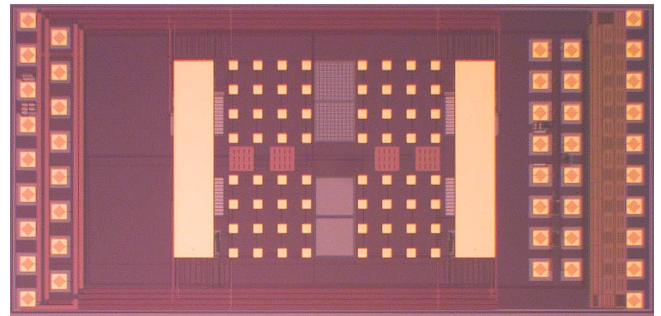


Fig. 11. Micrograph of the impedance-to-frequency converter test chip, showing the four electrode arrays with two large counter electrodes to both sides. The leftmost row of pads are supply and reference connections, the pads on the right hand side are the address and control bits and the digital output. Also visible are additional pads for various test structures.

of leakage in the switching matrix and the statistical mismatches introduced in the manufacturing process. The unavoidable variations of transistor parameters such as threshold voltage generally scale with the inverse of the transistor dimensions and become more pronounced in the weak inversion regime. In order to limit these variations, all transistors need to operate in the saturation region. To ensure this we designed the electrode current source as a chain of three cascode current mirrors, each with a scaling factor of 10:1, implementing a downscaling of a reference current by a factor of 1000 (see Fig. 10). Non-overlapping signals generated from the comparator output control the switches between current source and electrode.

3.2 Test chip

A test chip for the impedance-to-frequency converter was produced in a standard 0.35 μm 3.3 V CMOS technology (Austria Micro Systems). An additional lift-off process was performed in-house to process the surface electrodes consisting of a Ti-Pt-Au stack. Based on our simulations and the considerations outlined above, we chose an electrode size of 55 × 55 μm² and an inter-electrode distance of 100 μm. In total 64 sensing electrodes are located on the chip, organized in four arrays of 4 × 4, with the electrode closest to the chip center of each array accessible via a pad for testing purposes. Each of the electrodes can be addressed individually through a digital control interface. Two large counter electrodes keep the electrolyte at an externally supplied fixed potential. A chip photograph is shown in Fig. 11.

4 Measurement results

For the measurements with cells, the chip was mounted in a CPGA package and the bond wires were sealed with an epoxy resin. A small polystyrene dish was then mounted on top to act as a liquid reservoir. The biasing of the chip was

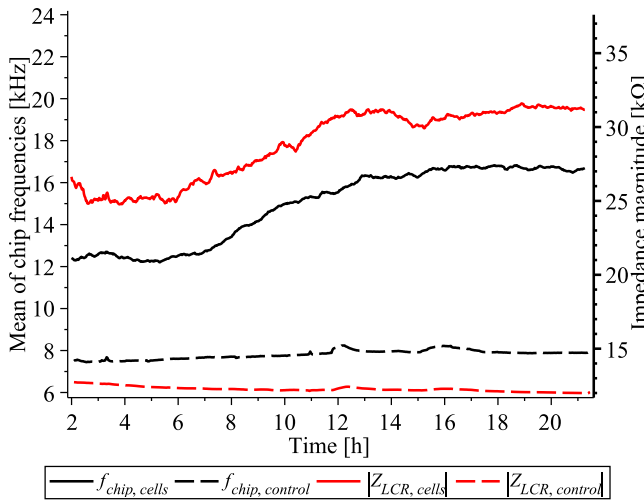


Fig. 12. Cell growth on the sensor chip captured with our impedance-to-frequency converter (black solid line, left axis) and actual impedance at 10 kHz measured simultaneously via a LCR meter connected to on-chip electrodes (red solid line, right axis). Also shown are data from a control experiment without cells (dashed lines).

adjusted for an electrode current of 70 nA. For comparison to the output of our impedance-to-frequency converter, we also connected a Hewlett Packard 4284A LCR meter to the chip, allowing us to record the actual impedance of the four center electrodes and at the same time measure the remaining 60 electrodes with the on-chip circuitry. A multifunction I/O box attached to a PC was used to output the digital address bits, supply power to the chip and to evaluate the frequency-modulated digital output.

To verify the functionality of the sensor system, we seeded cells on our test chip (1 million V79 cells in 2 ml of Dulbecco's Modified Eagle Medium), placed the chip with its support PCB in an incubator at 37°C and recorded the output frequencies of the impedance-to-frequency converters for each electrode, along with the impedance measured by the LCR meter on the four center electrodes.

In Fig. 12, the mean output frequency of our circuit for all sensing electrodes during this experiment is represented by the black curve. The red curve shows the impedance magnitude of the center electrodes as measured by the LCR meter. At the beginning of the plot, the cells have just settled on the chip from suspension, but have not yet attached to the substrate. In the following hours, they spread out and connect to neighboring cells, forming a confluent monolayer (Wegener et al., 2000). This is accompanied by an increase in impedance, which both curves show in good agreement.

The next day, the measurement was briefly interrupted and the formation of a tight cell coverage confirmed visually. The chip was then placed in the incubator again and the measurement continued. As can be seen in Fig. 13, the cells were not disturbed by this interruption and the signals stabilized at

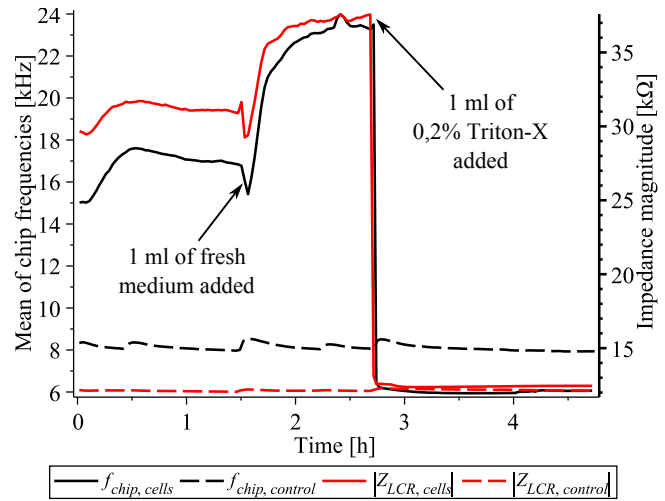


Fig. 13. Continuation of the experiment shown in Fig. 12. Cell reactions to the addition of fresh medium and later to the addition of the detergents Triton-X 100 are clearly visible.

their previous values within one hour. We then exchanged 1 ml of the used medium with an equal amount of fresh medium at room temperature. This caused a short dip of both curves, which we interpret as a temperature shock reaction, followed by a longer rise, which could be explained by the supply of oxygen and fresh nutrients by the new medium. When we repeated the identical experiment without cells as a control (dashed lines), no significant reaction could be observed, confirming that the effect was caused by the cells.

After allowing for the signals to stabilize, we again exchanged 1 ml of the used medium with 1 ml of medium containing 0.2 % Triton-X 100, a detergent which kills cells by destroying their membrane. An immediate drop of the impedance down to the base level of the control experiment followed as the cells died off and detached from the chip.

During the whole experiment, the changes of the mean chip frequency and the impedance measured by the LCR meter show high correlation, confirming the viability of our impedance-to-frequency converter for cell adhesion measurement. The slight discrepancies can be sufficiently explained by the different physical measurement locations on the chip and the nonlinearity of the relation between impedance magnitude and chip output frequency.

5 Conclusions

The evaluation of cell adhesion by impedance measurements can give valuable information about cell reactions and is thus an important element for a water quality biosensor. To harness the advantages of CMOS integration for such a sensor, we developed a model of the impedance under study, comprising contributions of the electrode and the cells. Using a combination of analytical and numerical techniques, this

allowed us to predict the nature and magnitude of the cellular impedance. An integrated impedance-to-frequency converter circuit was developed based on these results, allowing for a straightforward digital readout of cell adhesion data while taking into account the electrochemical limitations of the allowed currents and voltages. Experiments with cells proved the functionality of the measurement system.

References

- Bousse, L.: Whole cell biosensors, *Sensors and Actuators B*, 34, 270–275, doi:10.1016/S0925-4005(96)01906-5, 1996.
- Braun, D. and Fromherz, P.: Fluorescence Interferometry of Neuronal Cell Adhesion on Microstructured Silicon, *Physical Review Letters*, 81, 5241, doi:10.1103/PhysRevLett.81.5241, 1998.
- Ehret, R., Baumann, W., Brischwein, M., Schwinde, A., Stegbauer, K., and Wolf, B.: Monitoring of cellular behaviour by impedance measurements on interdigitated electrode structures, *Biosensors and Bioelectronics*, 12, 29–41, doi:10.1016/0956-5663(96)89087-7, 1997.
- Franks, W., Schenker, I., Schmutz, P., and Hierlemann, A.: Impedance characterization and modeling of electrodes for biomedical applications, *Biomedical Engineering, IEEE Transactions on*, 52, 1295–1302, doi:10.1109/TBME.2005.847523, 2005.
- Lo, C. M., Keese, C. R., and Giaever, I.: Impedance analysis of MDCK cells measured by electric cell-substrate impedance sensing., *Biophys. J.*, 69, 2800–2807, 1995.
- Ragheb, T. and Geddes, L.: The polarization impedance of common electrode metals operated at low current density, *Annals of Biomedical Engineering*, 19, 151–163, doi:10.1007/BF02368466, 1991.
- Ritter, M., Lang, F., Grübl, G., and Embacher, H. G.: Determination of cell membrane resistance in cultured renal epithelial (MDCK) cells: effects of cadmium and mercury ions, *Pflügers Archiv European Journal of Physiology*, 417, 29–36, doi:10.1007/BF00370765, 1990.
- Urdapilleta, E., Bellotti, M., and Bonetto, F. J.: Impedance analysis of cultured cells: A mean-field electrical response model for electric cell-substrate impedance sensing technique, *Physical Review E (Statistical, Nonlinear, and Soft Matter Physics)*, 74, 041908–11, doi:10.1103/PhysRevE.74.041908, 2006.
- Wegener, J., Keese, C. R., and Giaever, I.: Electric Cell-Substrate Impedance Sensing (ECIS) as a Noninvasive Means to Monitor the Kinetics of Cell Spreading to Artificial Surfaces, *Experimental Cell Research*, 259, 158–166, doi:10.1006/excr.2000.4919, 2000.